Impact of the Linker on the Electronic and Luminescent Properties of Diboryl Compounds: Molecules with Two $BMes_2$ Groups and the Peculiar Behavior of 1,6-$(BMes_2)_2$pyrene

Shu-Bin Zhao,[†] Philipp Wucher,[†] Zachary M. Hudson,[†] Theresa M. McCormick,[†] Xiang-Yang Liu,[†] Suning Wang,*[,†] Xiao-Dong Feng,[‡] and Zheng-Hong Lu[‡]

Department of Chemistry, Queen's University, Kingston, Ontario, K7L 3N6, Canada, and Department of Materials Sciences and Engineering, University of Toronto, Toronto, Ontario, M5S 3E5, Canada

Received September 3, 2008

To investigate the impact of the linker on the electronic and photophysical properties of diboryl compounds, three new diboryl compounds that contain two $BMes_2$ groups (Mes = mesityl) have been synthesized, including a planar 1,6-$(BMes_2)_2$pyrene (**1**), a V-shaped bis(*p*-$BMes_2$phenyl)diphenylsilane (**4**), and a U-shaped 1,8-bis(*p*-$BMes_2$phenyl)naphthalene (**5**). For comparison, two previously known compounds, *p*-$(BMes_2)_2$benzene (**3**) and 1,8-bis(*p*-$BMes_2$-biphenyl)naphthalene (**6**), were also investigated. The aromatic linkers in these molecules have been found to have a dramatic impact on the electron-accepting ability and Lewis acidity of the diboryl compounds through their distinct steric and electronic properties. Compound **1** has the most positive reduction potential ($E_{1/2}^{red1} = -1.81$ V, relative to $FeCp_2^{0/+}$), while **5** has the most negative reduction potential ($E_{1/2}^{red1} = -2.34$ V). All compounds are blue emitters with considerable variation of emission energy and efficiencies (e.g., $\lambda_{em} = 446$, 402, 395 nm, $\Phi = \sim 1.0$, 0.17, ~ 1.0 for **1**, **4**, and **5**, respectively), and each displays a distinct and selective response toward fluoride ions. Upon addition of fluoride ions, compound **1** displays an unusual red shift and an on−off response in both absorption and fluorescent spectra. By comparing the behavior of **1** to that of the monoboryl compound 1-$BMes_2$pyrene (**2**) and **3**, and with TD-DFT computations on **1** and its fluoride adducts **1F** and $\mathbf{1F_2}$, it has been found that the peculiar response of **1** toward fluoride ions is caused by the dominance of pyrene π orbitals at the HOMO level of **1F** and the relatively low-energy charge transfer from the pyrene ring to the three-coordinate boron center in **1F**. The crystal structures of **2**, **4**, $\mathbf{1F_2}$, and $\mathbf{5F_2}$ were determined by X-ray diffraction analyses. The potential use of compound **1** as either a blue emitter or a bifunctional emitter in OLEDs has been demonstrated by the successful fabrication of double- and triple-layer electroluminescent devices.

Introduction

Conjugated triarylboron systems are well known to be effective as fluorescent emitters, charge transport materials in organic light emitting diodes,[1−7] and highly selective sensors for fluoride ions.[8−23] These promising applications have recently generated interest in molecules with multiple boron centers that may serve as better anion sensors or emitters/electron transport materials in OLEDs. Electronic effects are known to play a key role in the chemistry of triarylboron centers; for example, we have recently reported a 2,2′-bipy-linked diboryl molecule, 5,5′-bis(dimesitylboron)-2,2′-bipy (B2bpy), that displays greatly enhanced Lewis acidity due to the electronegative pyridine linker.[21] In addition, the geometry of the linker is of key importance. For example, we have recently observed that a U-shaped diboryl molecule, 1,8-di(*p*-dimesitylborylbiphenyl)-naphthalene, binds to fluoride with a binding constant similar to those of the corresponding monoboron compounds.[22] However, Gabbai and co-workers have shown that when two triarylboron centers are attached directly to the 1,8-positions of naphthalene, the two boron centers can "chelate" to fluoride ions, giving a molecule with an exceptionally high affinity toward fluoride.[10] Most recently, Müllen and co-workers have observed an unusual spectral red shift in a large conjugated diboryl system on addition of fluoride ions,[24] differing from

* Corresponding author. E-mail: wangs@chem.queensu.ca.
[†] Queen's University.
[‡] University of Toronto.

(1) Noda, T.; Shirota, Y. *J. Am. Chem. Soc.* **1998**, *120*, 9714.
(2) Shirota, Y. *J. Mater. Chem.* **2005**, *15*, 75.
(3) Noda, T.; Ogawa, H.; Shirota, Y. *Adv. Mater.* **1999**, *11*, 283.
(4) Shirota, Y.; Kinoshita, M.; Noda, T.; Okumoto, K.; Ohara, T. *J. Am. Chem. Soc.* **2000**, *122*, 1102.
(5) Jia, W. L.; Bai, D. R.; McCormick, T.; Liu, Q. D.; Motala, M.; Wang, R.; Seward, C.; Tao, Y.; Wang, S. *Chem.−Eur. J.* **2004**, *10*, 994.
(6) Jia, W. L.; Moran, M. J.; Yuan, Y. Y.; Lu, Z. H.; Wang, S. *J. Mater. Chem.* **2005**, *15*, 3326.
(7) Wakamiya, A.; Mori, K.; Yamaguchi, S. *Angew. Chem., Int. Ed.* **2007**, *46*, 4237.
(8) Yamaguchi, S.; Shirasaka, T.; Akiyama, S.; Tamao, K. *J. Am. Chem. Soc.* **2002**, *124*, 8816.
(9) Yamaguchi, S.; Akiyama, S.; Tamao, K. *J. Am. Chem. Soc.* **2001**, *123*, 11372.
(10) Solé, S.; Gabbaï, F. P. *Chem. Commun.* **2004**, 1284.
(11) Melaimi, M.; Gabbaï, F. P. *J. Am. Chem. Soc.* **2005**, *127*, 9680. (e) Chiu, C. W.; Gabbaï, F. P. *J. Am. Chem. Soc.* **2006**, *128*, 14248.
(12) Hudnall, T. W.; Melaimi, M.; Gabbaï, F. P. *Org. Lett.* **2006**, *8*, 2747.
(13) Lee, M. H.; Agou, T.; Kobayashi, J.; Kawashima, T.; Gabbaï, F. P. *Chem. Commun.* **2007**, 1133.
(14) Lee, M. H.; Gabbaï, F. P. *Inorg. Chem.* **2007**, *46*, 8132.
(15) Hudnall, T. W.; Gabbaï, F. P. *J. Am. Chem. Soc.* **2007**, *129*, 11978.
(16) Dorsey, C. L.; Jewula, P.; Hudnall, T. W.; Hoefelmeyer, J. D.; Taylor, T. J.; Honesty, N. R.; Chiu, C.-W.; Schulte, M.; Gabbaï, F. P. *Dalton Trans.* **2008**, 4442.
(17) Hudnall, T. W.; Kim, Y.-M.; Bebbington, M. W. P.; Bourissou, D.; Gabbaï, F. P. *J. Am. Chem. Soc.* **2008**, *130*, 10890.

10.1021/om800856g CCC: $40.75 © 2008 American Chemical Society
Publication on Web 11/19/2008

Chart 1

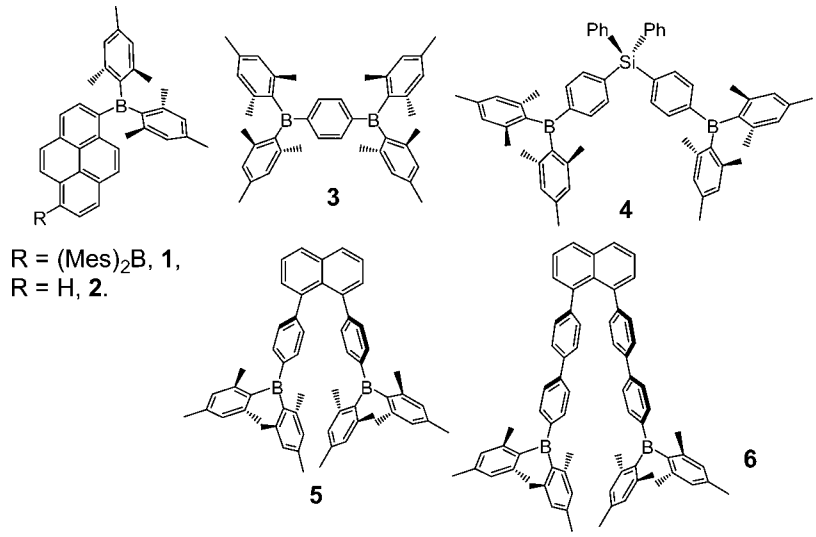

the blue shift that is typically observed.[21−23] Clearly, the electronic properties and the geometry of the linker have a significant impact on the Lewis acidity and the fluorescent response of polyboron compounds toward anions such as fluorides. To have a better understanding of the impact of the linker on the electronic and photophysical properties of diboryl molecules, we have extended our investigation to a series of new diboryl molecules with various linkers and distinct molecular shapes, as shown in Chart 1. As examples of linear or planar conjugated diboryl molecules, we examined 1,6-bis(dimesitylboron)pyrene (B2pyrene, **1**) and compared this to the monoboron-substituted pyrene, 1-(dimesitylboron)pyrene (B1pyrene, **2**), and the previously known *p*-$(BMes_2)_2$benzene,[28] **3**. Pyrene is known to be a highly efficient blue fluorescent emitter in solution, but not suitable for applications in OLEDs due to its tendency to produce excimer emission.[25−27] Decoration of pyrene by sterically bulky groups has been shown to be highly effective in reducing excimer emission,[27] making **1** a potentially attractive candidate for use in OLEDs. Furthermore, in contrast to the electronegative 2,2′-bipy linker, pyrene is a large electron-rich conjugated π system, which may lead to interesting properties in its diboryl derivative. We have also investigated a series of compounds in which the two boron centers do not lie in direct conjugation: the flexible diphenylsilane derivative **4** and the naphthyl-linked compounds **5** and **6**. Our investigations have produced some interesting and unexpected findings, the details of which are presented herein.

Experimental Section

All reactions were performed under N_2 with standard Schlenk techniques unless otherwise noted. All starting materials were purchased from Aldrich Chemical Co. and used without further purification. DMF, THF, Et_2O, and hexanes were purified using an Innovation Technology Co. solvent purification system. CH_2Cl_2 was freshly distilled over P_2O_5 prior to use. Deuterated solvents were purchased from Cambridge Isotopes and were used as received without further drying. NMR spectra were recorded on Bruker Avance 400 or 500 MHz spectrometers. High-resolution mass spectra were obtained from a Waters/Micromass GC-TOF EI-MS spectrometer, which was internally calibrated before use. 1,6-dibromopyrene,[29] 1,4-bis(dimesitylboryl)benzene (**3**)[28] *p*-bromophenyldimesitylborane,[5] and 1,8-bis(4-dimesitylborylbiphen-4′-yl)naphthalene[22] (**6**) were prepared according to previously reported procedures.

Cyclic voltammetry was performed using a BAS CV-50W analyzer with a scan rate of 500 to 4 V/s and a typical concentration of 5 mg of analyte in 3.0 mL of DMF using 0.10 M tetrabutylammonium hexafluorophosphate (TBAP) as the supporting electrolyte. A conventional three-compartment electrolytic cell consisting of a Pt working electrode, a Pt auxiliary electrode, and a Ag/AgCl reference electrode was employed using the ferrocene/ferrocenium couple as the internal standard ($E^{1/2}$ = 0.55 V). UV−vis spectra were recorded on an Ocean Optics UV−visible spectrometer. Excitation and emission spectra were recorded on a Photon Technologies International QuantaMaster model C-60 spectrometer. Emission lifetimes were measured on a Photon Technologies International Phosphorescent spectrometer (Time-Master C-631F) equipped with a xenon flash lamp and digital emission photon multiplier tube using a band pathway of 5 nm for excitation and 2 nm for emission.

Synthesis of 1,6-bis(dimesitylboryl)pyrene, 1. To a stirred THF (40 mL) solution of 1,6-dibromopyrene (0.40 g, 1.1 mmol) at −78 °C was added dropwise, via syringe, a *n*-BuLi solution (1.6 M) (1.44 mL, 2.3 mmol) over 10 min. The resulting light yellow solution was stirred for 1 h at −78 °C, and an Et_2O (15 mL) solution of dimesitylboron fluoride (0.72 g, 90%, 2.4 mmol) was then slowly added. After stirring at −78 °C for 1 h, the reaction mixture was warmed to ambient temperature and stirred overnight, affording a

(18) Sundararaman, A.; Venkatasubbaiah, K.; Victor, M.; Zakharov, L. N.; Rheingold, A. L.; Jäkle, F. *J. Am. Chem. Soc.* **2006**, *128*, 16554.
(19) Parab, K.; Venkatasubbaiah, K.; Jäkle, F. *J. Am. Chem. Soc.* **2006**, *128*, 12879.
(20) Jäkle, F. *Coord. Chem. Rev.* **2006**, *250*, 1107.
(21) Sun, Y.; Ross, N.; Zhao, S.-B.; Huszarik, K.; Jia, W. L.; Wang, R. Y.; Wang, S. *J. Am. Chem. Soc.* **2007**, *129*, 7510.
(22) Liu, X. Y.; Bai, D. R.; Wang, S. *Angew. Chem., Int. Ed.* **2006**, *45*, 5475.
(23) Bai, D. R.; Liu, X. Y.; Wang, S. *Chem.−Eur. J.* **2007**, *13*, 5713.
(24) Zhou, G.; Baumgarten, M.; Müllen, K. J. Am. Chem. Soc. ASAP article, published online (Aug 20, 2008).
(28) (a) Kaim, W.; Schulz, A. *Angew. Chem., Int. Ed. Engl.* **1984**, *23*, 615. (b) Schulz, A.; Kaim, W. *Chem. Ber.* **1989**, *122*, 1863.
(25) Mikroyannidis, J. A.; Fenenko, L.; Adachi, C. *J. Phys. Chem. B* **2006**, *110*, 20317.
(26) Kim, Y. H.; Yoon, D. K.; Lee, E. H.; Ko, Y. K.; Jung, H.-T. *J. Phys. Chem. B* **2006**, *110*, 20836.
(27) Wu, K.-C.; Ku, P.-J.; Lin, C.-S.; Shih, H.-T.; Wu, F.-I.; Huang, M.-J.; Lin, J.-J. *Adv. Funct. Mater.* **2008**, *18*, 67.
(29) (a) Suenaga, H.; Nakashima, K.; Mizuno, T.; Takeuchi, M.; Hamachi, I.; Shinkai, S. *J. Chem. Soc., Perkin Trans.1* **1998**, 1263. (b) Grimshaw, J.; Trocha-Grimshaw, J. *J. Chem. Soc., Perkin Trans. 1* **1972**, 1622.

yellow suspension. An aqueous solution (20 mL) of NH_4Cl (0.26 g) was added and stirred for 30 min. After separation of the aqueous layer, the organic suspension was concentrated and the residue was purified by flash chromatography on silica gel using $CHCl_3$ as the eluent to afford compound **1** as a yellow powder, which was further purified by recrystallization with acetone (0.41 g, 53% yield). ^{1}H NMR (500 MHz, CD_2Cl_2): δ 8.21 (d; ^3J = 9 Hz; 2H, pyrene), 8.09 (d; ^3J = 8 Hz; 2H, pyrene), 7.95 (d; ^3J = 8 Hz; 2H, pyrene), 7.87 (d; ^3J = 9 Hz; 2H, pyrene), 6.87 (s, 8H, B(*Mes*)$_2$), 2.35 (s, 12H, *p*-CH_3 of B(*Mes*)$_2$), 1.56 (s, 24H, *o*-CH_3 of B(*Mes*)$_2$), ppm. ^{13}C NMR could not be obtained due to the poor solubility of **1**. HRMS: calcd for $C_{52}H_{52}B_2Na$ $[M + Na]^+$ *m/z* 721.4152, found 721.4153. Anal. Calcd for $C_{52}H_{52}B_2$: C 89.40, H 7.50. Found: C 88.78, H 7.40.

Synthesis of 1-(Dimesitylboryl)pyrene, 2. To a stirred THF (40 mL) solution of 1-bromopyrene (0.40 g, 1.43 mmol) at −78 °C was added dropwise, via syringe, a *n*-BuLi solution (1.6 M) (0.94 mL, 1.5 mmol) over 10 min. The resulting light yellow solution was stirred for 1 h at −78 °C, and an Et_2O (10 mL) solution of dimesitylboron fluoride (0.48 g, 90%, 1.6 mmol) was then slowly added. After stirring at −78 °C for 1 h, the reaction mixture was warmed to ambient temperature and stirred overnight, affording a yellow solution. After the removal of the solvent, the residue was purified by flash chromatography on silica gel using hexanes as the eluent to afford compound **2** as a yellow solid, which was then recrystallized by slow evaporation of its CH_2Cl_2/hexanes (1:1) solution to give yellow crystals (0.39 g, 61% yield). ^{1}H NMR (500 MHz, $CDCl_3$, 25 °C): δ 8.21 (d; ^3J = 8.0 Hz; 1H, pyrene), 8.19 (d; ^3J = 9.5 Hz; 1H, pyrene), 8.16 (d; ^3J = 7.0 Hz; 1H, pyrene), 8.15 (d; ^3J = 9.0 Hz; 1H, pyrene), 8.14 (d; ^3J = 7.5 Hz; 1H, pyrene), 8.09 (d; ^3J = 9.0 Hz; 1H, pyrene), 8.03 (d; ^3J = 8.0 Hz; 1H, pyrene), 8.01 (m; 1H, pyrene), 7.90 (d; ^3J = 9.5 Hz; 1H, pyrene), 6.85 (s; 4H, B(*Mes*)$_2$), 2.36 (s; 6H, *para*-CH_3 of B(*Mes*)$_2$), 1.99 (s; 12H, *orth*-CH_3 of B(*Mes*)$_2$) ppm. ^{13}C NMR: δ 144.95 (br), 144.41(br), 141.06, 139.53, 135.22, 133.92, 133.39, 131.71, 131.34, 129.16, 128.91, 128.00, 127.98, 127.75, 126.20, 125.83, 125.72, 125.35, 125.06, 124.82, 23.08, 21.72 ppm. Anal. Calcd for $C_{34}H_{31}B$: C 90.66, H 6.94. Found: C 90.83, H 6.67.

Synthesis of Di(*p*-dimesitylborylphenyl)diphenylsilane, 4. To a stirred THF (30 mL) solution of di(*p*-bromophenyl)diphenylsilane (0.320 g, 0.65 mmol) at −78 °C was added dropwise, via syringe, a *n*-BuLi solution (1.6 M in hexanes) (0.90 mL, 1.44 mmol) over 5 min. The resulting light yellow solution was stirred for 1 h at −78 °C, and a THF (20 mL) solution of dimesitylboron fluoride (0.46 g, 90%, 1.55 mmol) was then slowly added. After stirring at −78 °C for 1 h, the reaction mixture was allowed to warm slowly to room temperature and stirred overnight, giving a yellow transparent solution. The solvent was then evaporated and the residue partitioned between CH_2Cl_2 (50 mL) and H_2O (50 mL). After separation, the aqueous layer was extracted with CH_2Cl_2 (30 mL × 3), and the combined organic layers then washed with saturated aqueous NaCl (50 mL). The organic layer was then dried ($MgSO_4$) and concentrated. The residue was purified by flash chromatography on silica gel using hexanes as the eluent to afford compound **4** as a white powder (0.29 g, 55% yield). ^{1}H NMR (500 MHz, $CDCl_3$): δ 7.51−7.60 (m; 8H), 7.48 (d; ^3J = 7.9 Hz; 4H), 7.41 (t; ^3J = 7.3 Hz; 2H, phenyl), 7.33−7.39 (m; 4H, phenyl), 6.81 (s; 8H, B(*Mes*)$_2$), 2.30 (s; 12H, *para*-CH_3 of B(*Mes*)$_2$), 2.01 (s, 24H, *ortho*-CH_3 of B(*Mes*)$_2$) ppm. ^{13}C NMR: δ 147.1, 141.7, 140.8, 138.7, 138.3, 136.3, 135.8, 135.0, 133.8, 129.7, 128.2, 128.1, 127.9, 23.4, 21.2 ppm. Anal. Calcd for $C_{60}H_{62}B_2Si$: C 86.53, H 7.50. Found: C 86.63, H 7.67.

Synthesis of 1,8-Di(*p*-dimesitylborylphenyl)naphthalene, 5. To a THF solution (30 mL) of *p*-bromophenyldimesitylborane (0.65 g, 1.6 mmol) at −78 °C was added dropwise, via syringe, a *n*-BuLi solution (1.6 M) (1.05 mL, 1.7 mmol). The resulting light yellow solution was stirred for 1 h at −78 °C, at which point anhydrous $ZnCl_2$ solid (0.24 g, 1.8 mmol) was added. After 1 h at −78 °C, the reaction mixture was warmed to ambient temperature. 1,8-diiodonaphthalene (0.30 g, 0.8 mmol) and $Pd(PPh_3)_4$ (0.13 g, 0.12 mmol) were then added successively to this solution, and the mixture was stirred at ambient temperature for 2 days. After the removal of the solvent, the residue was dissolved in CH_2Cl_2 (50 mL) and an aqueous Na_4EDTA solution (50 mL, 0.20 M, prepared from EDTA with 5 equiv of Na_2CO_3). The mixture was stirred for 30 min, and the aqueous layer was then separated and extracted with CH_2Cl_2 (2 × 50 mL). The organic layer was dried with Na_2SO_4 and concentrated, and the residue purified by flash chromatography on silica gel using hexanes/CH_2Cl_2 (1:5) as the eluent to afford compound **3** as a white solid (0.36 g, 58% yield). ^{1}H NMR (400 MHz, $CDCl_3$): δ 7.91 (dd; ^3J = 8.0 Hz; 2H, naphthalene), 7.54 (dd; ^3J = 8.4 Hz; 2H, naphthalene), 7.35 (m; 2H, naphthalene), 7.25 (d; ^3J = 8.0 Hz; 4H, bridging −Ph−), 7.07 (d; ^3J = 8.0 Hz; 4H, bridging −Ph−), 6.80 (s; 8H, B(*Mes*)$_2$), 2.32 (s; 12H *p*-CH_3 of B(*Mes*)$_2$), 1.92 (s; 24H, *o*-CH_3 of B(*Mes*)$_2$). ^{13}C NMR: δ 147.93, 141.53, 141.27, 140.73, 140.70, 138.31, 137.24, 135.51, 131.11, 129.51, 128.77, 128.20, 128.09, 125.34, 23.80, 21.22. HRMS: calcd for $C_{58}H_{58}B_2$ $[M]^+$ *m/z* 776.4725, found 776.4763. Anal. Calcd for $C_{58}H_{58}B_2$ C 89.69; H 7.53. Found: C 90.04; H 7.75.

Fabrication of Electroluminescent Devices. Two different EL devices have been produced using a K. J. Lesker OLED cluster tool with six high-vacuum process chambers: (A) ITO-CuPc (25 nm)/NPB (45 nm)/**1** (40 nm)/LiF(1 nm)-Al and (B) ITO-CuPc (25 nm)/NPB (45 nm)/**1** (40 nm)/TPBi (10 nm)/LiF (1 nm)-Al. All materials were deposited by vacuum on 2 in. × 2 in. ITO-coated glass substrates. The patterned ITO surface was sequentially cleaned in acetone, methanol, and deionized water, and with UV ozone treatment. All the testing devices have an active area of 2 × 1 mm^2. The base pressures of the organic and metalization chambers are 4×10^{-8} and 1.9×10^{-6} Torr, respectively. The pressures during the deposition process in the two chambers are lower than 4.6×10^{-6} Torr. The growth rates are ∼1.5 Å s^{-1} for organic materials, 0.1 Å s^{-1} for LiF, and ∼1.5 Å s^{-1} for aluminum. Luminance−current density−voltage (L-J-V) characteristics were determined in ambient atmosphere using a HP 4140B pA meter and a Minolta LS-110 m. The dwell time for each testing point is 2 s. EL spectra were recorded using an USB2000-UV−vis miniature fiber optic spectrometer.

Molecular Orbital Calculations. The Gaussian suite of programs (Gaussian 03)[30] employing density functional theory (DFT) including Becke's three-parameter hybrid methods with Lee−Yang−Par correlation functions (B3LYP) was used for all calculations. Crystal structures were used as the starting point for geometry optimizations where possible. For compounds where no crystal structure was available, the starting geometries were prepared by modifying optimized structures of similar compounds using Gaussview software. All compounds were fully optimized at the B3LYP/6-311G(d) level of theory. For compounds **1**, **1F**, **1F$_2$**, **2**, and **2F**, the six lowest singlet and triplet transition energies were calculated using time-dependent DFT calculations on the optimized structures, at the B3LYP/6-311G(d) level of theory.

X-ray Crystallographic Analysis. Single crystals of **2** and **4** were obtained from the slow evaporation of solvents (CH_2Cl_2/hexanes). Single crystals of **1F$_2$** and **5F$_2$** were obtained from slow evaporation of the CH_2Cl_2 solutions of **1** and **5**, respectively, in the presence of excess N(*n*-Bu)$_4$F. The crystals were mounted on glass fibers for data collection. Data were collected at either 180 K or ambient temperature on a Bruker Apex II single-crystal X-ray diffractometer with graphite-monochromated Mo Kα radiation, operating at 50 kV and 30 mA. The crystals of **2** and **4** belong to the triclinic space group $P\bar{1}$, while the crystals of **1F$_2$** and **5F$_2$** belong to the orthorhombic space group *Pbca* and *Pbcn*, respectively. No

(30) Frisch, M. J.; et al. *Gaussian 98* (Revision A.6); Gaussian, Inc.: Pittsburgh, PA, 1998.

Table 1. Crystal Data

	2	**4**	**1F$_2$**	**5F$_2$**
formula	$C_{34}H_{31}B$	$C_{60}H_{62}B_2Si$	$C_{84}H_{124}N_2B_2F_2$	$C_{45}H_{63}NFB$
fw	450.40	832.81	1221.47	647.77
space group	$P\bar{1}$	$P\bar{1}$	*Pbca*	*Pbcn*
a, Å	8.5670(9)	13.038(1)	19.6359(16)	18.9303(13)
b, Å	11.2119(12)	14.1669(11)	19.7648(17)	23.0165(15)
c, Å	13.7498(15)	14.6777(11)	22.7120(19)	19.0849(13)
α, deg	98.642(1)	67.266(1)	90	90
β, deg	103.914(1)	87.495(1)	90	90
γ, deg	98.317(1)	80.888(1)	90	90
V, Å^3	1244.7(2)	2468.6(3)	8814.5(13)	8315.5(10)
Z	2	2	4	8
$D_{calc,}$ g·cm^{-3}	1.202	1.120	0.920	1.035
T, K	180	180	180	298
μ, mm^{-1}	0.067	0.085	0.054	0.061
$2\theta_{max}$, deg	54.30	54.44	54.44	54.70
reflns measd	14 107	28 166	57 503	31 592
reflns used (R_{int})	5405(0.034)	10 804(0.040)	9727(0.062)	2570(0.044)
parameters	322	580	435	470
R [$I > 2\sigma(I)$]:	0.0538	0.0522	0.0789	0.0465
R_1[a]	0.1346	0.1222	0.2236	0.1228
wR_2[b]				
R (all data):	0.0949	0.0897	0.2211	0.0583
R_1[a]	0.1552	0.1410	0.2839	0.1337
wR_2[b]				
GOF on F^2	1.034	1.030	0.873	1.033

[a] $R_1 = \sum||F_o| - |F_c||/\sum|F_o|$. [b] $wR_2 = [\sum w[(F_o^2 - F_c^2)^2]/\sum[w(F_o^2)^2]]^{1/2}$, $w = 1/[\sigma^2(F_o^2) + (0.075P)^2]$, where $P = [\mathrm{Max}(F_o^2,0) + 2F_c^2]/3$.

significant decay was observed for all crystals. Data were processed using the Bruker SHELXTL software package (version 5.10) and are corrected for absorption effects. The structures were solved by direct methods. One of the *n*-butyl groups of the N(*n*-Bu)$_4^+$ cation in **5F$_2$** is disordered over two sites with an occupancy factor of ~50% for each site, which was modeled and refined successfully. The *n*-butyl groups in **1F$_2$** all display some degree of disordering; two of the disordered groups in **1F$_2$** were modeled and refined successfully. There are also disordered CH_2Cl_2 solvent molecules in the crystal lattice of **1F$_2$**, whose contributions to the structural data were removed using the Platon Squeeze algorithm.[31] All sufficiently ordered non-hydrogen atoms were refined anisotropically. The crystal data and selected bond lengths and angles are provided in Tables 1 and 2, respectively. Complete crystal data can be found in the Supporting Information.

Results and Discussion

Syntheses and Characterizations. The syntheses of three new diboryl compounds **1**, **4**, and **5** were accomplished using reactions shown in Scheme 1. For comparative study, the monoboron compound **2** was also synthesized. The syntheses of **1**, **2**, and **4** are straightforward and can be achieved via lithiation of the corresponding dibromo compound, followed by the addition of $BMes_2F$ as depicted in Scheme 1. The synthesis of **5** is quite challenging due to steric effects. Standard Suzuki−Miyaura coupling methods did not produce compound **5** in good yield, though the Negishi method[32] employing an organozinc(II) intermediate and $Pd(PPh_3)_4$ as the catalyst produced compound **5** in modest yield. All four compounds were fully characterized by ^{1}H and ^{13}C NMR and elemental analyses. Crystals suitable for X-ray diffraction analyses were obtained for compounds **2** and **4**, and their crystal structures are shown in Figures 1 and 3, respectively.

Table 2. Selected Bond Lengths (Å) and Angles (deg)

Compound **2**			
B(1)−C(17)	1.571(3)	C(17)−B(1)−C(1)	119.82(17)
B(1)−C(1)	1.572(3)	C(17)−B(1)−C(26)	120.41(17)
B(1)−C(26)	1.581(3)	C(1)−B(1)−C(26)	119.76(17)
Compound **4**			
Si(1)−C(19)	1.8692(19)	C(19)−Si(1)−C(1)	108.65(9)
Si(1)−C(1)	1.873(2)	C(19)−Si(1)−C(7)	110.93(9)
Si(1)−C(7)	1.873(2)	C(1)−Si(1)−C(7)	110.01(9)
Si(1)−C(13)	1.8861(19)	C(19)−Si(1)−C(13)	106.48(8)
B(1)−C(16)	1.572(3)	C(1)−Si(1)−C(13)	108.55(8)
B(1)−C(34)	1.577(3)	C(7)−Si(1)−C(13)	112.09(9)
B(2)−C(22)	1.565(3)	C(16)−B(1)−C(34)	119.86(17)
B(1)−C(25)	1.579(3)	C(16)−B(1)−C(25)	117.26(17)
B(2)−C(52)	1.573(3)	C(34)−B(1)−C(25)	122.88(16)
B(2)−C(43)	1.580(3)	C(22)−B(2)−C(52)	121.86(17)
		C(22)−B(2)−C(43)	117.09(17)
		C(52)−B(2)−C(43)	121.05(17)
Compound **1F$_2$**			
F(1)−B(1)	1.475(4)	F(1)−B(1)−C(19)	103.2(2)
B(1)−C(19)	1.656(4)	F(1)−B(1)−C(10)	110.0(2)
B(1)−C(10)	1.659(5)	C(19)−B(1)−C(10)	109.4(3)
B(1)−C(1)	1.672(5)	F(1)−B(1)−C(1)	104.3(2)
		C(19)−B(1)−C(1)	118.4(2)
		C(10)−B(1)−C(1)	111.0(2)
Compound **5F$_2$**			
B(1)−C(13)	1.640(6)	F(1)−B(1)−C(10)	103.6(3)
B(1)−C(22)	1.657(7)	F(1)−B(1)−C(13)	108.3(4)
B(1)−F(1)	1.494(5)	C(10)−B(1)−C(13)	109.0(4)
B(1)−C(10)	1.638(6)	F(1)−B(1)−C(22)	99.6(3)
C(1)−C(2)	1.345(6)	C(10)−B(1)−C(22)	116.9(4)
C(1)−C(6)	1.401(6)	C(13)−B(1)−C(22)	117.7(4)
C(2)−C(3)	1.391(6)	C(3)−C(4)−C(7)	112.6(5)
C(3)−C(4)	1.373(6)	C(5)−C(4)−C(7)	128.5(6)
C(4)−C(5)	1.436(5)	C(4′)−C(5)−C(4)	128.0(8)
C(4)−C(7)	1.502(6)	C(4)−C(5)−C(6)	116.0(4)
C(5)−C(6)	1.444(8)	C(1′)−C(6)−C(1)	117.0(9)
		C(1)−C(6)−C(5)	121.5(5)

As shown in the crystal structure for compound **2**, the steric interactions between the H atom on C(13) of the pyrene moiety and the mesityl group on the boron center cause the noncoplanarity between the trigonal BC_3 plane (defined by B(1), C(1), C(17), and C(26) atoms) and the plane of the pyrene linker (dihedral angle = 43.7°). In addition, the C(17) phenyl ring and the C(26) phenyl rings are nearly perpendicular to the pyrene plane, as evidenced by the large dihedral angles of 90.0° and 80.3°, respectively. Hindered rotation around the B−C bond by the mesityl groups was confirmed by variable-temperature ^{1}H NMR spectra of **2**, as shown in Figure 2. At 220 K, all *meta*-H atoms and all methyl groups of the $BMes_2$ display distinct chemical shifts. The rotation barriers of the B−C(mesityl) bond for the two mesityl groups in **2** were determined to be 11.6 and 12.2 kcal mol^{-1}, respectively. These are notably greater than that observed in the previously reported BNPB system,[33] in which the $BMes_2$ group is attached to a phenyl ring (10.3 kcal mol^{-1}), consistent with the greater steric interactions imposed by the pyrene ring in **2**. In the crystal lattice of **2**, the pyrene portion of the molecule stacks with extended $\pi-\pi$ interactions, as shown in Figure 1. Although the crystal structure of **1** was not determined by X-ray diffraction, based on the structure of **1F$_2$** and molecular modeling, $\pi-\pi$ stacking interactions between the pyrene rings are unlikely in **1** due to steric blocking by the two $BMes_2$ groups. The separation distance

(31) (a) Spek, A. L. *Acta Crystallogr.* **1990**, *A46*, C34. (b) Spek, A. L. *PLATON*, A Multipurpose Crystallographic Tool; Ultrecht University: Ultrecht, The Netherlands, 2006.

(32) King, A. O.; Okukado, N.; Negishi, E.-i. *Chem. Commun.* **1977**, 683.

(33) Jia, W. L.; Feng, X. D.; Bai, D. R.; Lu, Z. H.; Wang, S.; Vamvounis, G. *Chem. Mater.* **2005**, *17*, 164.

(34) Fiedler, J.; Zališ, S.; Klein, A.; Hornung, F. M.; Kaim, W. *Inorg. Chem.* **1996**, *35*, 3039.

(35) Okada, K.; Kawata, T.; Oda, M. *Chem. Commun.* **1995**, 233.

Scheme 1

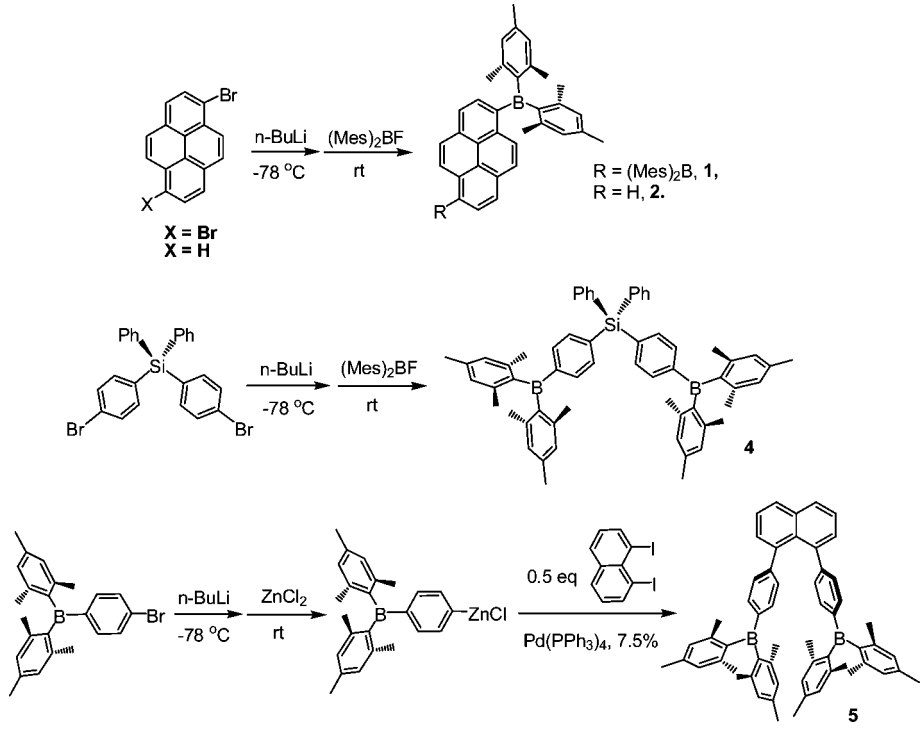

between the two boron centers in **1** is ~9.06 Å, based on the structure optimized by DFT calculations.

The Si(1) atom in compound **4** has a typical tetrahedral geometry with normal Si−C bond distances, and the two boron centers are 9.97 Å apart. The two trigonal BC_3 planes are much closer to coplanarity with the phenyl linkers than those in compound **1** with pyrene, showing dihedral angles of 22.6° for B(1) and 28.6° for B(2) between the BC_3 plane and the phenyl linker. The dihedral angles between the mesityl rings and the phenyl linker are 69.6°, 67.3°, 73.8°, and 72.5°, respectively, much smaller than those in **2**, but similar to previously reported compounds where the $BMes_2$ group is attached to a phenyl ring.[21,23,24,33] This is consistent with the decreased steric congestion in **4**. ^{1}H NMR data also indicate that **4** has a rotational barrier around the B−C(mesityl) bond similar to that of BNPB.

For compound **5**, molecular modeling shows that the two boron centers are ~6.5 Å apart, much closer than those in **4** and **6** (~10 Å); hence, greater steric interactions between the two $BMes_2$ groups are likely present in **5**. Nonetheless, ^{1}H NMR data support that the rotation barrier around the B−C(mesityl) bond in **5** is similar to that in **4** and **6**.

Electrochemical Properties. To examine the impact of the linker on the electron-accepting ability of these boron compounds, we recorded the CV diagrams of compounds **1**−**5**. Compound **1** has a very poor solubility in polar solvents. As a result, the intensity of the CV peak of **1** is barely above the background level. Nonetheless, as shown in Figure 4, two reduction peaks are clearly visible and reproducible for compound **1**. The reduction potentials of compounds **1**−**5** along with compound **6** are listed in Table 3. Among the linearly conjugated molecules, molecule **1** has the most positive $E_{1/2}^{red1}$ at −1.81 V (vs $FeCp_2^{+/0}$), while **2** has the most negative $E_{1/2}^{red1}$ at −2.03 V. It is noteworthy that both these potentials are considerably more positive than those of previously reported monoboron compounds attached to either a benzene or biphenyl (typically $E_{1/2}^{red1} \leq -2.20$ V),[23,33−35] though not as positive as in B2bpy ($E_{1/2}^{red1} = -1.69$ V, $E_{1/2}^{red2} = -2.07$ V, $\Delta E_{1/2} = 0.38$ V).[20]

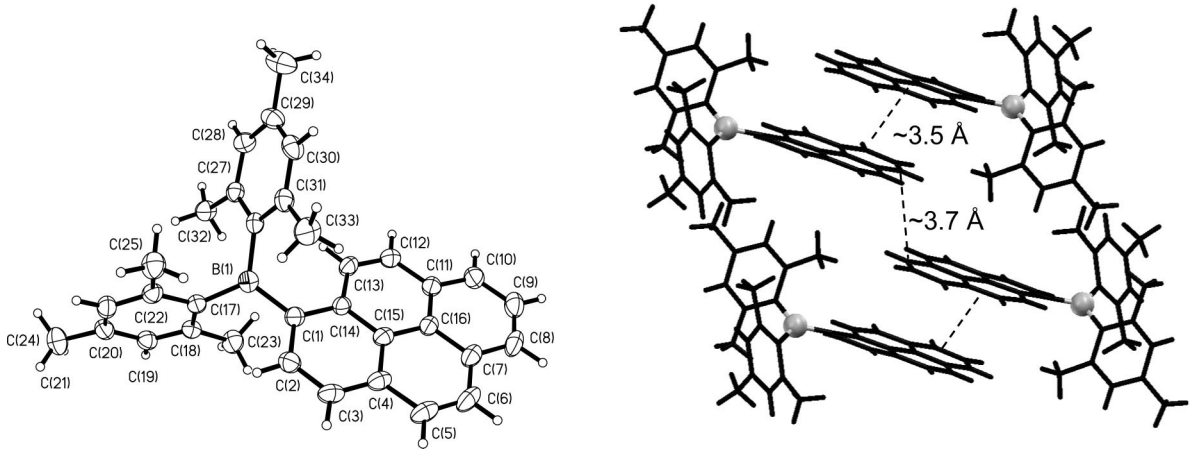

Figure 1. Left: Diagram showing the structure of **2** with 50% thermal ellipsoids and labeling schemes. Right: Diagram showing intermolecular π stacking of the pyrene rings in the crystal lattice of **2**.

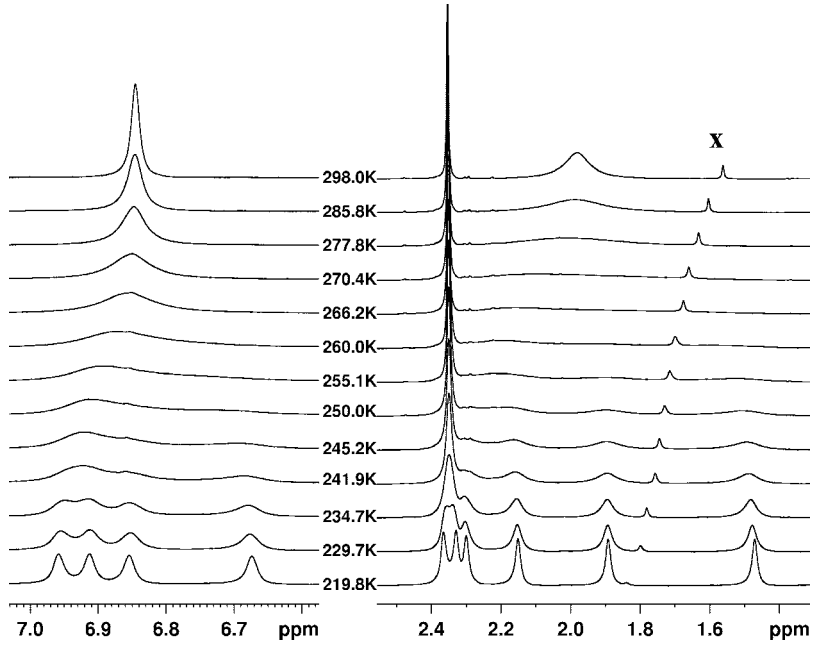

Figure 2. Variable-temperature ^{1}H NMR spectra of **2** showing the chemical shifts of the *meta*-H atoms and methyl protons of the mesityl groups (CD_2Cl_2). The H_2O impurity is marked by "X".

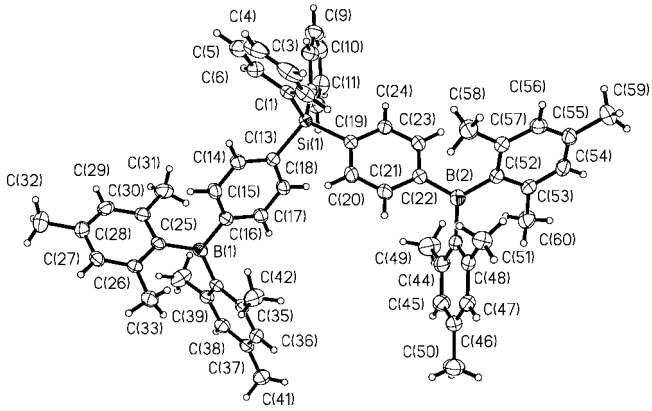

Figure 3. Diagram showing the structure of **4** with 50% thermal ellipsoids and labeling scheme.

Thus, it can be concluded that the electron-accepting ability of **1** is enhanced by the presence of both a second boron center and the large conjugate ring of the pyrene group. The fact that the $\Delta E_{1/2}$ of 0.35 V in **1** is similar to that of B2bpy supports that the pyrene ring promotes a strong electronic communication between the two boron centers as the bpy does. For the monoboron pyrene molecule **2**, a second reversible reduction peak at −2.66 V was observed that can be attributed to the reduction of the pyrene ring (nonsubstituted pyrene has a reduction peak at −2.58 V in DMF). For **3**, because the two boron centers are much closer to each other (∼6.0 Å) than those in **1** (∼9.1 Å), a greater electronic communication between the two boron centers is expected. However, molecule **3** has an $E_{1/2}^{red1}$ at −1.90 V, which is between those of **1** and **2**, with $\Delta E_{1/2}$ (0.33 V) being slightly less than that of **1** (0.35 V). Furthermore, both reduction peaks displayed by **3** have a poor reversibility, an indication that **3** is much less stable toward reduction compared to **1** and **2**. Thus, the pyrene linker is more effective in enhancing the electron-accepting ability and electronic communication of the boron centers than the phenyl linker.

Table 3. Reduction Potentials[a] of Compounds 1−6

	1	2	3	4	5	6
$E_{1/2}^{red1}$	−1.81	−2.03	−1.90	−2.28 (shoulder)	−2.34	−2.28
$E_{1/2}^{red2}$	−2.16	−2.66	∼−2.28	−2.43	−2.63	−2.68

[a] Measured in DMF, relative to $FeCp_2^{0/+}$ ($E_{1/2}^{ox}$ = 0.55 V).

The V-shaped diboryl molecule **4** displays a reduction peak at −2.43 V and a shoulder peak at −2.28 V, as shown in Figure 4, presumably due to the successive reduction of the two boron centers. The presence of two reduction peaks, albeit not well resolved, supports the presence of a weak electronic com-

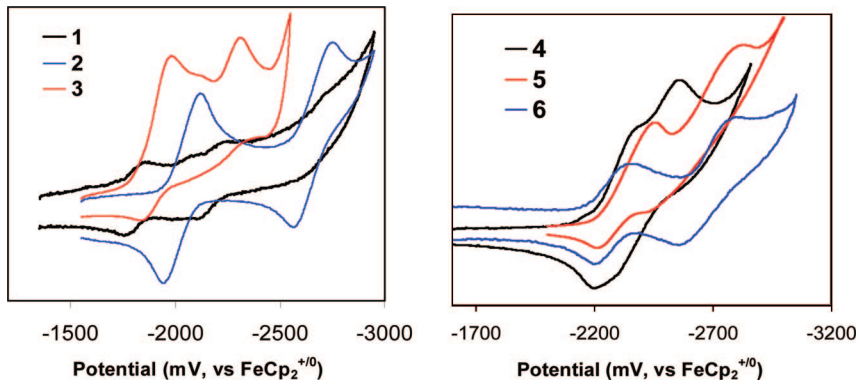

Figure 4. CV diagrams of **1**−**3** (left) and **4**−**6** (right) recorded in DMF with scan rates of 1 or 2 V.

Table 4. Absorption and Emission Data for 1, 2, 4, and 5

compound	absorption,[c] nm (ϵ, M^{-1} cm^{-1}), CH_2Cl_2	emission, CH_2Cl_2, 298 K	
		λ_{max}, nm	Φ_{PL}
1	426 (59400), 401 (36500), 342 (15900), 301 (32000), 246 (77600)	446	~1.0[a]
2	398 (33800), 385 (30200), 325 (17300), 310 (17700), 294 (25000), 245 (75300)	427	~1.0[a]
4	318 (27700), 272 (24400), 230 (49600)	402	0.17[b]
5	338 (48100), 278 (20500), 232 (65600)	395	~1.0[b]

[a] Using 9,10-diphenylanthracene as the standard. [b] Using anthracene as the standard. [c] 1.0×10^{-5} M, 298 K.

Table 5. Luminescence Data for Compound 1, 2, 4, and 5 in Different Solvents[a]

	excitation wavelength (λ_{ex}, nm)				emission wavelength (λ_{em}, nm)			
	hexanes	toluene	CH_2Cl_2	DMF	hexanes	toluene	CH_2Cl_2	DMF
1	427	428	420	426	432	436	446	439
2	399	400	399	399	401	413	427	424
4	332	332	331	332	359	373	402	406
5	343	351	349	351	380	388	395	409

[a] [M] = 1.0×10^{-5} mol/L, 298 K.

munication between the two boron centers in **4**. The naphthyl-linked diboryl molecule **5** has two reduction peaks at −2.34 and −2.63 V, respectively, attributable to the reduction of the two boron centers as well. Although the boron separation distances and the $E_{1/2}^{red1}$ values in **4** and **6** are similar, the $E_{1/2}^{red2}$ value of **6** is much more negative than that of **4**, indicative of the presence of a greater electronic communication between the boron centers in **6**. This is likely due to the rigid naphthyl linker in **6**, which forces strong $\pi-\pi$ stacking interactions of the two biphenyl groups and imposes a greater electrostatic repulsive force between the two boron anions. Such "negative cooperativity" is related to the phenomenon observed by Jäkle and coworkers in anion binding of conjugated diboryl systems,[18,36] but is previously unknown in nonconjugated systems.

Compared to the conjugated molecules **1**−**3**, the nonconjugated molecules **4**−**6** are clearly weaker electron acceptors with much more negative $E_{1/2}^{red1}$ values. π-Conjugation with the $BMes_2$ group is therefore most effective in enhancing the electron-accepting ability of the B center. Among the directly conjugated molecules reported here, the diborylpyrene molecule is the strongest electron acceptor.

Absorption and Luminescent Properties. Compounds **1**−**5** have intense and distinct absorption bands in the 230−450 nm region, as shown in Figure 5. Most notable is compound **1**, which has a strong absorption band in the visible region (λ_{max} = 426 nm), while the same band is absent in the spectrum of **2**. Hence, this low-energy absorption band in **1** is clearly associated with the presence of the two conjugated $BMes_2$ groups, and because of it, compound **1** has a bright yellow color in solution, while all other compounds are either colorless or light yellow (compound **2**).

Compounds **1**, **2**, **4**, and **5** are all fluorescent with λ_{max} = 446, 427, 402, and 395 nm in CH_2Cl_2, respectively. With the exception of the V-shaped molecule **4**, which has an emission quantum efficiency of 17%, all the new molecules have a quantum efficiency of nearly 100%, measured using either 9,10-diphenylanthracene or anthracene as the standard (Table 4). The fluorescent spectra of all molecules show some degree of dependence on the solvent polarity, with the V-shaped molecule **4** displaying the largest shift (hexane to CH_2Cl_2, 43 nm red shift) and the diboryl pyrene molecule **1** the smallest shift (hexane to CH_2Cl_2, 14 nm red shift), while their absorption spectra show little dependence on solvents, as shown in Table 5. Although the emission spectral red shift with solvent polarity by the molecules **1**, **2**, **4**, and **5** is not as dramatic as that displayed by the previously reported donor−acceptor type of boron molecules, they do suggest that the excited state of these molecules[22,23,33] is likely polarized. In the case of the diborylpyrene molecule **1**, no excimer emission typical of pyrene was observed over a concentration range of 10^{-4} to 10^{-7} M, which can be credited to the two $BMes_2$ groups that block intermolecular interactions between two pyrene units. For **2**, excimer emission appears to be evident in a high concentration solution (~10^{-3} M; see Supporting Information), consistent with the π-stacking interactions among pyrene rings revealed by the crystal structure of **2**. With concentrations ≤ ~10^{-4} M (higher concentration is not possible due to poor solubility), the emission spectrum of **2** is dominated by the $\pi \rightarrow \pi^*$ transition band. The behavior of compound **5** is similar to that of **6**, though the emission maximum of **6** is red-shifted (λ_{max} = 414 nm in CH_2Cl_2) and has a greater solvent dependence (hexane to CH_2Cl_2, 20 nm red shift). In fact, DFT calculations for **6** established that the HOMO level is dominated by the naphthyl ring and the LUMO by the empty p orbitals of the two boron centers.[22] Hence, the solvent-dependent fluorescence of **5** and **6** can be explained by a polarized electronic transition from the naphthyl to the boron center. Due to the longer biphenyl group in **6**, this molecule will be more polarized than **5** in the excited state, and thus more responsive to changes in solvent polarity. DFT calculations for molecule **4** revealed that the HOMO level consists of two degenerate orbitals, each with contributions primarily from the mesityl groups on one boron leg only, while each of the doubly degenerate LUMOs possesses large contributions from both

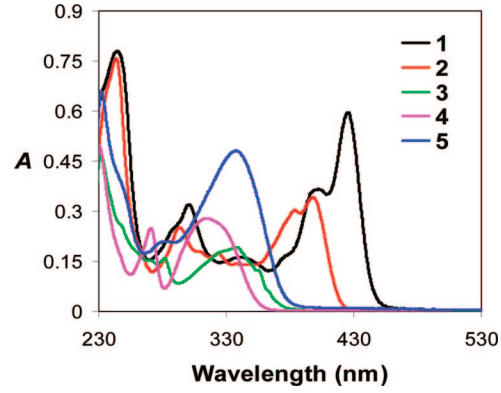

Figure 5. UV−vis spectra of **1**−**5** in CH_2Cl_2 (1.0×10^{-5} M).

(36) Sundararaman, A.; Victor, M.; Varughese, R.; Jäkle, F. *J. Am. Chem. Soc.* **2005**, *127*, 13478.

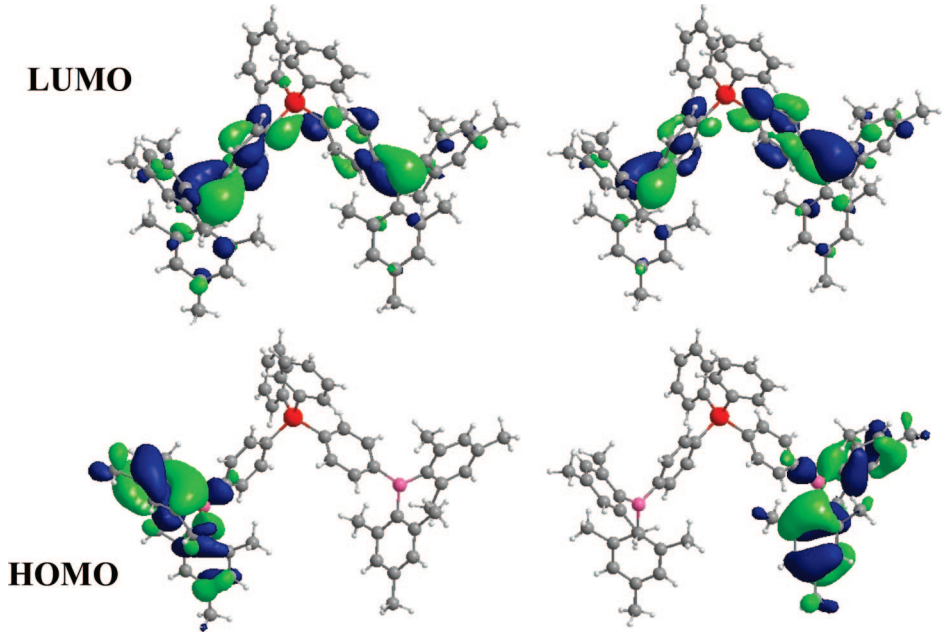

Figure 6. Diagrams showing the HOMO and LUMO levels of **4** calculated by DFT plotted with an isocontour value of 0.03 au.

boron centers (Figure 6). Hence the lowest electronic transition in **4** can be considered as a charge transfer from the mesityl groups on one leg to the boron centers on both, creating a highly polarized excited state. To further understand the photophysical properties and the Lewis acidity of molecules **1**, **2**, **4**, and **5**, we examined the interaction of fluoride anions with these molecules.

Interactions with Fluoride Anions. The response of the boron compounds toward fluoride ions was examined in both absorption and emission modes. The addition of fluorides to **2** and **3** causes a blue shift of both absorption and emission spectra as well quenching of fluorescent emission, which is typical for linearly conjugated triarylboron molecules.[21−23] The UV−vis and fluorescent titration diagrams of **2** are shown in Figure 7. For **3**, these diagrams are provided in the Supporting Information. The Stern−Volmer plots shown in Figure 8 for both **2** and **3** are nearly identical, indicating that both molecules have a similar affinity toward fluoride.

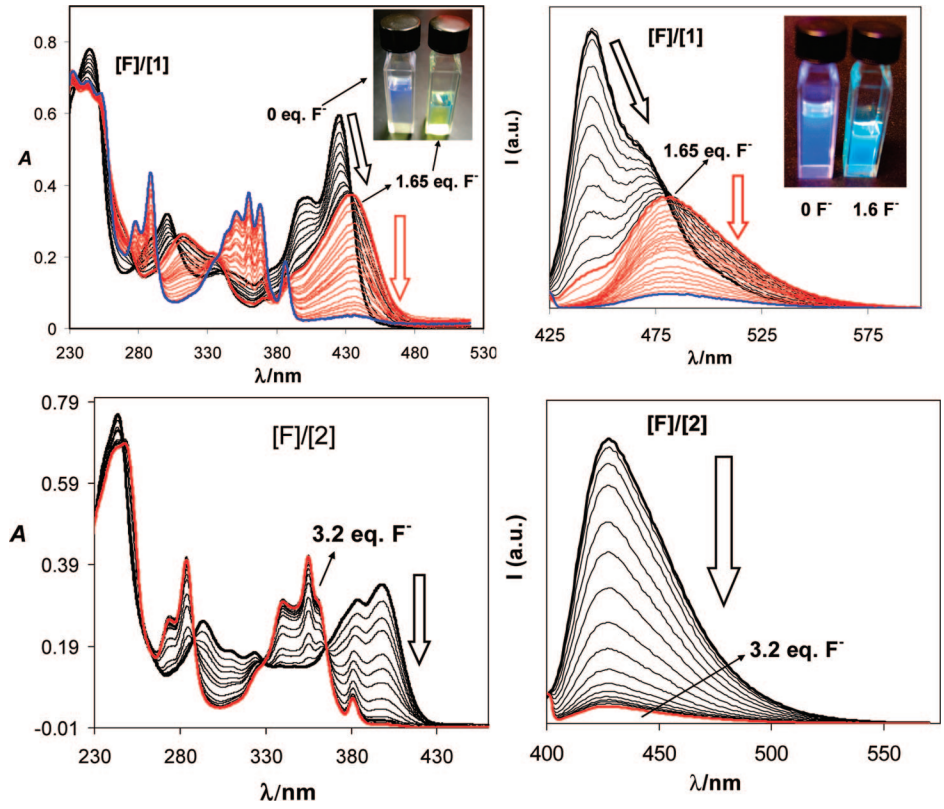

Figure 7. UV−vis (left) and fluorescent titration diagrams of **1** (top) and **2** (bottom) in CH_2Cl_2 (1.0×10^{-5} M) by NBu_4F. Top, inset: photographs taken under ambient light and UV light showing the effect of the addition of 1.65 equiv of F^- to the solution of **1** at 1.0×10^{-5} M.

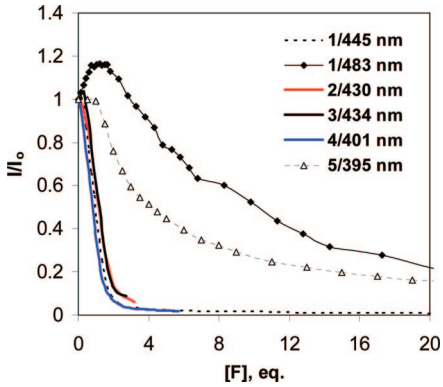

Figure 8. Stern−Volmer plots of **1**−**5** titration by NBu_4F.

The response of the diboryl pyrene molecule **1** toward fluoride ions is both complex and surprising, as shown in Figure 7. In both UV−vis absorption spectra and the emission spectra, the addition of F^- causes a distinct red shift. The absorption at 426 nm and emission at 445 nm lose intensity until about 1.7 equiv of F^- is added, as a new absorption at 436 nm and emission at 483 nm appear. Beyond this point, the new absorption and emission peaks lose intensity with increasing concentration of fluorides, and the saturation point is reached after ∼30 equiv of TBAF is added. These spectral red shifts with <1.7 equiv of fluorides cause the solution of **1** to change color from yellow to bright yellow-green, as shown in Figure 7, and the emission color to change from dark blue to sky blue. Further titration to the saturation point causes a near-complete loss in emission color. These unusual color changes and the complex behavior of **1** toward fluoride ions may be attributed to the sequential binding of fluoride ions to the first and second boron centers, forming **1F** and $\mathbf{1F_2}$, respectively, and the coexistence of **1**, **1F**, and $\mathbf{1F_2}$ in solution. Hence, the response of **1** toward F^- can be described as sequential turn on and off. The Stern−Volmer plot of **1** for the quenching of the emission peak at 445 nm (Figure 8) shows that the binding strength of **1** with the first fluoride ion is somewhat similar to that of **2** (<2 equiv of F^- is needed to completely quench the initial emission peak). However, the further binding of **1F** to form $\mathbf{1F_2}$ is much weaker than that of **2** to **2F**, as evidenced by the slow quenching of the peak at 483 nm of **1** shown in Figure 8, which again can be attributed to the negative cooperativity caused by electrostatic repulsion between two $BMes_2F$ centers. It is noteworthy that after the addition of excessive fluoride ions the UV−vis titration spectral change of **1F** to $\mathbf{1F_2}$ and **2** to **2F** becomes similar, supporting that **1F** and **2** share a common electronic structure. Nonetheless, the absorption and emission spectra of **1F** are considerably red-shifted, compared to those of **2**. The ability of molecule **1** to bind to two fluoride ions is confirmed by the isolation of the difluoride adduct $\mathbf{1F_2}$ and its crystal structure shown in Figure 9, where the central pyrene ring is well protected by the sterically bulky $BMes_2F$ groups. Since the diborylbenzene **3** does not show a similar red shift with the addition of fluoride, the pyrene linker clearly plays a key role in the peculiar response of **1** toward fluoride.

Both the V-shaped **4** and the U-shaped **5** undergo fluorescent quenching with the addition of fluoride ions. The data for compound **4** are shown in Figure 10, and the data for **5** are provided in the Supporting Information. The key difference between these two molecules is that molecule **4** has a much greater affinity toward fluoride ions than does **5**, as shown by the fluorescent Stern−Volmer plots in Figure 8. UV−vis titrations of **4** and **5** by fluorides show a spectral blue shift and similar Stern−Volmer plots. The binding strength of **4** with fluoride ions is in fact on the same order of magnitude as that of **2** and **3**. In contrast, molecule **5** binds much more weakly toward fluoride due to the strong steric interactions between

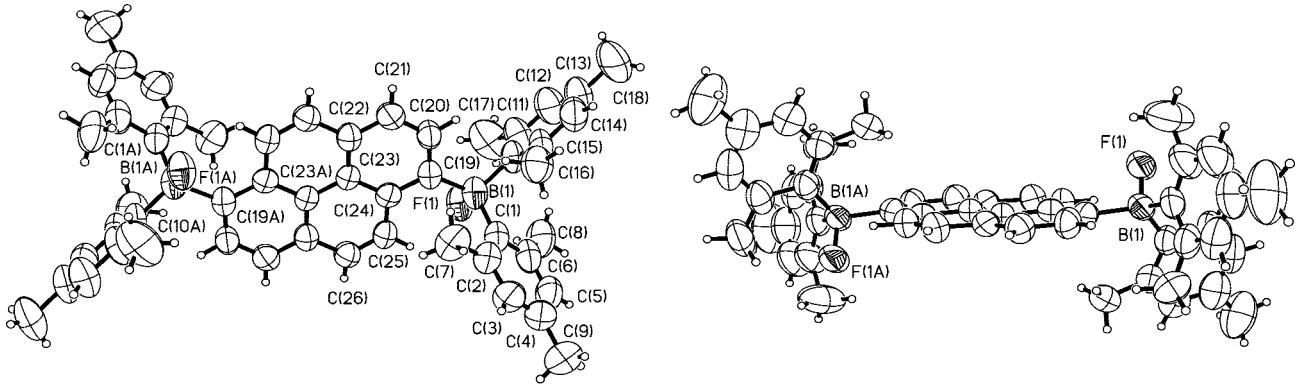

Figure 9. Diagrams showing the structure of $\mathbf{1F_2}$ with labeling schemes, top view (left) and side view (right). The cations are omitted.

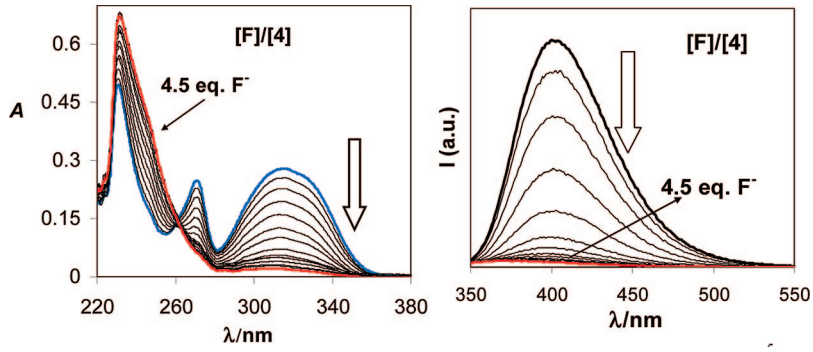

Figure 10. UV−vis (left) and fluorescent titration diagrams of **4** in CH_2Cl_2 (1.0×10^{-5} M) by NBu_4F.

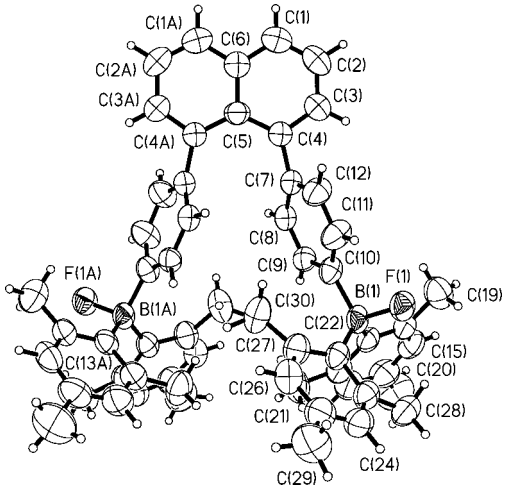

Figure 11. Diagram showing the structure of $\mathbf{5F_2}$ with labeling schemes. The cations are omitted.

the two boron centers, as confirmed by the crystal structure of the difluoride adduct $\mathbf{5F_2}$, shown in Figure 11. The two boron centers in $\mathbf{5F_2}$ are 7.36 Å apart, compared to 6.5 Å in **5**. Thus, the change of the boron center geometry from trigonal planar to tetrahedral noticeably increases congestion in this rigid molecule.

TD-DFT Calculations for 1, 2, and Their Fluoride Adducts. To further understand the peculiar UV−vis and fluorescent response of compound **1** toward fluoride ions, we carried out TD-DFT calculations on compound **1** and its monofluoride and difluoride adducts. For comparison, we also performed calculations on the monoboron compound **2** and its monofluoride adduct. The calculation results show that the lowest energy transition is dominated by the HOMO−LUMO transition for all compounds. The calculated HOMO−LUMO energy gaps along with the optical energy gaps obtained experimentally from UV−vis spectra in CH_2Cl_2 are provided in Table 6. The computational results confirm that the HOMO−LUMO gap of **1F** is smaller than that of **1** and $\mathbf{1F_2}$, supporting that the absorption and emission spectral red shift of **1** after the addition of <1.7 equiv of F^- is indeed due to the formation of the monofluoride adduct. The MO diagrams for **1** shown in Figure 12 illustrate that the pyrene ring plays a key role in the electronic transitions of **1**, **1F**, and $\mathbf{1F_2}$. For **1**, both the HOMO and LUMO are π orbitals of the pyrene ring with significant contributions from the B centers at the LUMO level. This is in sharp contrast to the diborylbenzene molecule **3**, in which the HOMO level has contributions predominantly from

Table 6. HOMO−LUMO Enery Gaps for 1 and 2 and Their F^- Adducts

compd	MO HOMO−LUMO gap (eV)	transition	optical energy gap (eV), CH_2Cl_2
1	2.81	$\pi_{pyr} \rightarrow \pi_{pyr}^*$ (with B contributions)	2.79
1F	2.50	$\pi_{pyr} \rightarrow p_\pi$ (B) (with pyrene contributions)	2.61
$\mathbf{1F_2}$	3.41	$\pi_{pyr} \rightarrow \pi_{pyr}^*$	3.14
2	3.03	$\pi_{pyr} \rightarrow \pi_{pyr}^*$ (with B contributions)	2.95
2F	3.41	$\pi_{pyr} \rightarrow \pi_{pyr}^*$	3.18

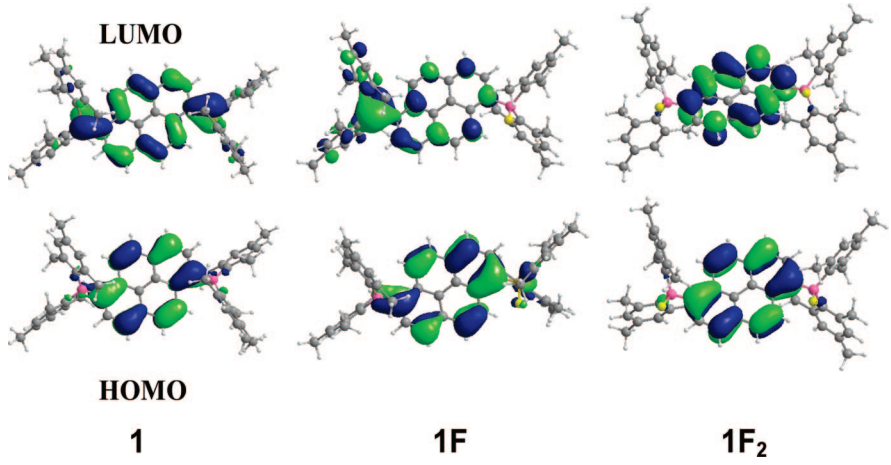

Figure 12. Diagrams showing the HOMO and LUMO orbitals of **1** and its fluoride adducts calculated by TD-DFT, plotted with an isocontour value of 0.03 au.

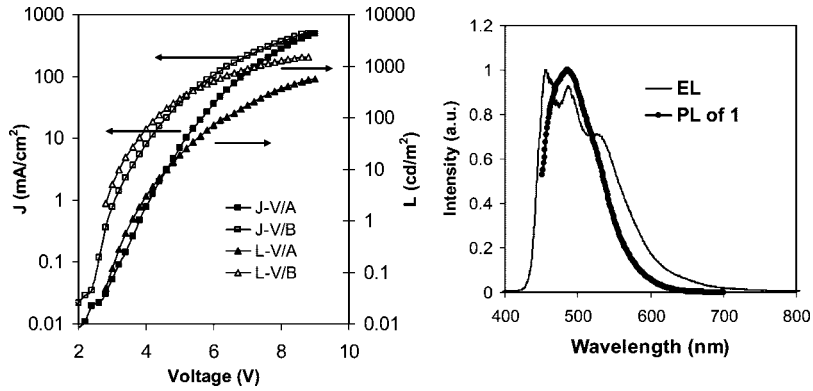

Figure 13. Left: The J-L-V plots. Right: The EL and PL plots.

the mesityl groups. For **1F**, the HOMO is again a pyrene π orbital, but the LUMO level is dominated by the p_π orbital of the trigonal boron center with significant contributions from the pyrene π system. Therefore, the lowest electronic transition in **1F** is charge transfer between pyrene and the trigonal boron center, which is lower in energy than the $\pi \rightarrow \pi^*$ transition in **1**. The low HOMO−LUMO gap of the pyrene ring and its relatively high HOMO level are clearly responsible for such a low-energy charge transfer. In the case of $\mathbf{1F_2}$, the HOMO and LUMO involve the pyrene ring only, and as a result, this molecule has the largest HOMO−LUMO gap. The HOMO and LUMO diagrams of **2** and **2F** resemble the corresponding ones in **1F** and $\mathbf{1F_2}$, consistent with the similar UV−vis and emission spectral change of **1** and **2** when excess fluorides are added. The HOMO energy level of **1F** is however much higher than that of **2** due to the destabilization by the $BMes_2F$ group, thus causing **1F** to have a much smaller HOMO−LUMO gap than **2**. Hence, the peculiar response of **1** toward fluoride ions can be explained by the involvement of the pyrene ring that leads to the low-energy charge transfer transition of **1F**. The spectral red shift of **1** to **1F** resembles the behavior of the BPPB molecule reported by Müllen et al., in which two dimesitylboron groups are connected by a long linear pentaphenyl linker and the extended π-conjugation is re-enforced by two spiro rings,[24] leading to a low HOMO−LUMO gap and a high HOMO level, similar to that observed in **1**.

Electroluminescent Devices of 1. Between the conjugated molecules **1** and **2**, compound **1** is the most promising for use in OLEDs because of its blue emission with a high emission quantum efficiency, its relatively high electron affinity (LUMO ≈ -2.9 V), and its lack of excimer emission. We therefore decided to evaluate the performance of **1** as either an emitter or a bifunctional electron transport emitter in electroluminescent devices. Two types of EL devices [A (ITO-CuPc/NPB/**1**/LiF-Al) and B (ITO-CuPc/NPB/**1**/TPBi/LiF-Al)] were fabricated, where CuPc and NPB (*N*,*N*′-diphenyl-*N*,*N*′-bis(1-naphthalenyl)-1,1′-biphenyl-4,4′-diamine) are employed as the hole injection and hole transport layers, respectively. In device B, the well-known electron transport material[37] TPBi (1,3,5-tris(*N*-phenylbenzimidazol-2-yl)benzene) was used. Both devices emit a sky blue light with a turn-on voltage of ~4 V and similar EL spectra, as shown in Figure 13. The EL spectra from both devices are very broad with three peaks, at 460, 490 and 535 nm, respectively, covering nearly the entire 400−700 nm region. The EL spectrum matches reasonably well with the PL spectrum of **1** in the solid state, although it is much broader with well-resolved peaks. It is possible that exciplex emission may be produced between the layers of NPB and compound **1**, contributing to the long-wavelength EL emission band. As shown by the J-V and L-V diagrams in Figure 13, the triple-layer device B is brighter and much more efficient than device A, with A and B having a maximum brightness of 571 and 1523 cd/m^2, respectively. The current efficiency at 100 cd/m^2 is ~0.75 cd/A for B, which is modest for a blue EL device. Therefore, compound **1** can be used as a bifunctional material in OLEDs, as demonstrated by the double-layer device A, though an additional electron transport layer is necessary in order to achieve a bright EL device, as illustrated by device B.

(37) Chen, C. H.; Shi, J. *Coord. Chem. Rev.* **1998**, *171*, 161.

Conclusions

On the basis of the results of this investigation and our earlier investigation on B2bpy, we can conclude the following for diboryl systems where two $BMes_2$ groups are linked together by an aromatic linker. (1) Electron-accepting ability: Linearly conjugated diboryl molecules are most favorable in achieving high electron affinity due to the direct participation of the empty p_π orbital of the boron center in the extended conjugate system that lowers the energy of the LUMO level. Extended large π systems such as pyrene or electronegative π systems such as bipyridine are most effective in stabilizing the radical anions of the reduced diboryl molecules and are thus most promising as electron transport materials. (2) Lewis acidity and fluoride binding: Although Lewis acidity is clearly related to the electron affinity of the boron center, our study has shown that steric interactions can also play a key role in a diboryl compound's ability to bind to fluoride ions. The linearly conjugated molecules **1** and **2** have a much more positive $E_{1/2}^{red1}$ than the V-shaped molecule **4**, yet all three molecules have a similar binding strength with fluoride ions. The steric interactions between the protons of the mesityls and the pyrene ring in **1** and **2** clearly hinder the boron binding of fluoride ions. Compound **5** has a reduction potential similar to that of **4**, but displays the lowest affinity to fluoride ions due to unfavorable steric interactions between the two boron legs in **5**. Hence, to achieve a strong acceptor for fluoride ions, linear linkers such as bipy, which are strong electron acceptors, promote strong π conjugation with boron centers, and do not impose great steric barriers to fluoride binding should be used. (3) Luminescence: Because of the conjugation of the boron center with the aromatic linker, the linker group has a great impact on the emission efficiency of the diboryl molecules. Among the linear molecules, pyrene derivatives **1** and **2** are the brightest blue emitters, much brighter than b2py and **3**, a feature clearly caused by the pyrene ring. Similarly, the naphthyl-linked molecules **5** and **6** also display nearly unit emission quantum efficiencies, while the V-shaped molecule **4** displays a much weaker emission quantum efficiency due to the sp^3-hybridized linker. Electronic interactions between the two aryl-boron legs in **5** and **6** may also play a role in their highly efficient emission.

Acknowledgment. We thank the Natural Sciences and Engineering Research Council of Canada for financial support.

Supporting Information Available: Stern−Volmer plots of UV−vis titrations of **1**−**5** with fluoride ions, UV−vis and fluorescent titration diagrams of **3** and **5**, UV−vis and fluorescent spectra of **1**, **2**, **4**, and **5** in various solvents, fluorescent spectra of compounds **1** and **2** in CH_2Cl_2 at various concentrations, complete variable-temperature ^{1}H NMR spectra of **2**, diagrams of the HOMO and LUMO of **2**, **2F**, and **3**, and complete crystal data for **2**, **4**, $\mathbf{1F_2}$, and $\mathbf{5F_2}$. This material is available free of charge via the Internet at http://pubs.acs.org.

OM800856G